IX International Conference on Particle-Based Methods
PARTICLES 2025
J. Bonet, M. Cremonesi, A. Franci, A. Gil (Eds)

DESCRIPTION OF AIR-DROPLET FLOW IN THE PROBLEM OF AIRCRAFT ICING MODELING

S. ALEKSIEIENKO[*], Z. SAZANISHVILI[†] AND V. NEKRASOV[*]

[*] Department of Technologies of Mechanical Engineering and Materials Science (TMEMS),
Dnipro University of Technology
49005 Dnipro, Ukraine
e-mail: aleksieienko.s.v@nmu.one, www.nmu.org.ua

[†] Engineering and Generative Design Department (EGD)
Dnipro University of Technology
49005 Dnipro, Ukraine
e-mail: sazanishvili.z.v@nmu.one, www.nmu.org.ua

Key words: Air-Droplet Flow, Polydisperse Eulerian Model, Lagrangian Trajectory Model, Homogeneous Model, CFD, UAV, Aircraft Icing.

Abstract. In-flight aircraft icing is a serious problem affecting flight safety and operational reliability. Atmospheric supercooled water droplets impinge on aircraft surfaces and freeze, forming ice, which can severely degrade aerodynamic performance and operational safety, potentially leading to a complete loss of control. Computational fluid dynamics is an important tool in the development of aircraft anti-icing systems, and modeling icing processes is a complex, interdisciplinary, and multi-physics task. This study presents approaches to describing the air-droplet incoming flow in aircraft icing modeling and analyzes the behavior of droplets interacting with an ice-covered aerodynamic surface. The Navier-Stokes equations coupled with the Spalart-Allmaras turbulence model are used to describe the motion of the carrier medium. The applicability of the polydisperse Eulerian, Lagrangian trajectory, and homogeneous models is analyzed for supercooled droplet dynamics. Numerical simulation of icing processes is performed using the control volume method, taking into account the conservation laws of mass, momentum, and energy. The analysis conducted in this work showed that the homogeneous model is appropriate for conditions near the phase transition point. The freezing of moisture that impinges on the aerodynamic surface is primarily governed by the temperature of the aerodynamic body and its heat exchange with the incoming flow. In cases where supercooled atmospheric droplets play a dominant role in the icing process, the Lagrangian trajectory model and the polydisperse Eulerian model are preferable for describing the air-droplet flow. The primary conclusion is that the polydisperse Eulerian model is preferable, as it best accounts for the characteristics of two-phase viscous compressible flow around bodies and the interaction of the carrier and liquid phases, making it the most promising approach for modeling aircraft icing. The results obtained can be used to ensure flight safety, design anti-icing systems, and investigate aviation accidents.

1 INTRODUCTION

The problem of aircraft icing in flight remains one of the most critical issues in modern aviation, as it directly affects aerodynamic performance, controllability, and flight safety. Traditional methods for modeling ice accretion, based on Lagrangian trajectory approaches, have several significant limitations. These include the assumption of incompressible incoming airflow and the neglect of its prior history; limited applicability at high flight speeds and for complex ice geometries or multibody configurations; challenges in implementation for three-dimensional cases; and the need to employ one-dimensional approximations and integral methods when calculating heat transfer. Moreover, these approaches do not allow for accurate evaluation of aerodynamic characteristics in the presence of ice deposits and surface roughness.

The development of modern numerical methods, particularly computational fluid dynamics (CFD), provides opportunities to overcome these limitations. Modeling icing in a fully three-dimensional framework is essential because two-dimensional approximations are insufficient for many aircraft components. These include swept wings, where three-dimensional effects appear near the wingtips; fuselage-wing junctions; tail surfaces; asymmetric nacelles; and air intakes. Accurate assessment of flow structures and ice formation mechanisms in these cases requires the use of comprehensive three-dimensional models.

This issue is especially relevant for small unmanned aerial vehicles (UAVs). Unlike large aircraft, which have substantial lift reserves and are equipped with certified anti-icing systems, small UAVs have limited aerodynamic margins and are highly sensitive to changes in surface geometry. Even minor ice accumulation can result in significant reductions in lift, increases in drag, and loss of stability. Typical operational conditions for small UAVs—low-altitude flights in the presence of supercooled droplets, drizzle, or rain near zero temperatures—further increase the risk of icing. In this context, numerical modeling of icing processes serves not only as a tool for risk assessment but also as a foundation for designing effective UAV anti-icing systems.

This paper examines the applicability of various models for simulating the dynamics of supercooled droplets, specifically polydisperse Eulerian, Lagrangian trajectory, and homogeneous models. The primary goal is to identify the most suitable approach for modeling aircraft icing, accounting for interactions between the carrier and dispersed phases in a two-phase viscous compressible flow. Special attention is given to the advantages of the polydisperse Eulerian model, highlighting its potential as a promising approach for further research in icing modeling and the development of UAV anti-icing systems.

2 DESCRIPTION OF EXTERNAL AIR-DROPLET FLOW

When modeling airflow containing supercooled water droplets in aircraft icing problems, three main approaches can theoretically be used: the polydisperse Eulerian model, the Lagrangian trajectory model, and the homogeneous model [1–3]. Each approach offers distinct advantages and limitations, depending on the degree of physical detail required, the computational resources available, and the specific characteristics of the icing scenario under consideration.

2.1 Homogeneous model

In the homogeneous model, moisture loss on a streamlined surface is driven by the temperature difference at the water film–vapor interface. This results from the balance between condensation of molecules impinging on the liquid surface (with partial reflection accounted for by the condensation coefficient) and the simultaneous evaporation of molecules leaving the surface. Condensation occurs when the number of captured molecules exceeds those released. Moisture loss is not limited to the leading edge of the profile. The unsteady flow of moist air and supercooled droplets, accounting for non-equilibrium condensation, can be described using gas dynamics equations that capture the mass, momentum, and energy exchange between phases [2–4]. In curvilinear coordinates, the non-stationary equations describing water vapor flow are expressed as follows:

$$\frac{\partial \hat{\mathrm{q}}}{\partial \tau}+\frac{\partial \hat{\mathrm{E}}}{\partial \xi}+\frac{\partial \hat{\mathrm{F}}}{\partial \eta}+\frac{\partial \hat{\mathrm{G}}}{\partial \zeta}+\hat{\mathrm{H}}=\frac{1}{\mathrm{Re}}\left(\frac{\partial \hat{\mathrm{R}}}{\partial \xi}+\frac{\partial \hat{\mathrm{S}}}{\partial \eta}+\frac{\partial \hat{\mathrm{T}}}{\partial \zeta}\right), \tag{1}$$

where

$$\hat{\mathrm{q}}=\frac{1}{J}\begin{bmatrix}\rho_g\\ \rho_g u\\ \rho_g v\\ \rho_g w\\ e_g\end{bmatrix},\quad \hat{\mathrm{E}}=\frac{1}{J}\begin{bmatrix}\rho_g U\\ \rho_g Uu+\xi_x p\\ \rho_g Uv+\xi_y p\\ \rho_g Uw+\xi_z p\\ \left(e_g+p\right)U\end{bmatrix},\quad \hat{\mathrm{F}}=\frac{1}{J}\begin{bmatrix}\rho_g V\\ \rho_g Vu+\eta_x p\\ \rho_g Vv+\eta_y p\\ \rho_g Vw+\eta_z p\\ \left(e_g+p\right)V\end{bmatrix},\quad \hat{\mathrm{G}}=\frac{1}{J}\begin{bmatrix}\rho_g W\\ \rho_g Wu+\zeta_x p\\ \rho_g Wv+\zeta_y p\\ \rho_g Ww+\zeta_z p\\ \left(e_g+p\right)W\end{bmatrix},$$

$$\hat{\mathrm{R}}=\frac{1}{J}\begin{bmatrix}0\\ \tau_{xx}\\ \tau_{xy}\\ \tau_{xz}\\ \beta_x\end{bmatrix},\quad \hat{\mathrm{S}}=\frac{1}{J}\begin{bmatrix}0\\ \tau_{xy}\\ \tau_{yy}\\ \tau_{yz}\\ \beta_y\end{bmatrix},\quad \hat{\mathrm{T}}=\frac{1}{J}\begin{bmatrix}0\\ \tau_{xz}\\ \tau_{yz}\\ \tau_{zz}\\ \beta_z\end{bmatrix},\quad \hat{\mathrm{H}}=-\frac{1}{J}\begin{bmatrix}-\rho\dot{m}\\ -\rho u\dot{m}\\ -\rho v\dot{m}\\ -\rho w\dot{m}\\ \rho\dot{m}\left(h_{fg}-h_t\right)\end{bmatrix}, \tag{2}$$

$$e_g=\rho\left[\varepsilon_g+\frac{1}{2}\left(u^2+v^2+w^2\right)\right].$$

The system of equations is closed by the equation of state for an ideal gas, given as:

$$p=\left(\gamma-1\right)\rho\varepsilon.$$

In the above relations: ρ_g – the vapor density; $\xi_x,\xi_y,\xi_z,\eta_x,\eta_y,\eta_z,\zeta_x,\zeta_y,\zeta_z,\mathrm{J}$ – the metric coefficients and the Jacobian of the coordinate transformation

$\xi = \xi(x, y, z, t), \eta = \eta(x, y, z, t), \zeta = \zeta(x, y, z, t)$; p – the pressure; e – the total energy; ε – the specific internal energy, with the subscript g indicating the vapor phase. The source term H accounts for the exchange of mass, momentum, and energy between phases. Within the source term $\dot{m}$ – the mass condensed per unit time, h_{fg} – the latent heat of phase transition, $\rho\dot{m}\left(h_{fg} - h_t\right)$ – the heat transferred during condensation, $\tau_{xx}, \tau_{xy}, \tau_{xz}, \tau_{yy}, \tau_{yz}, \tau_{zz}$ – the components of the stress tensor, $\beta_x, \beta_y, \beta_z$ – the components of the heat flux vector, and γ – the ratio of specific heats.

The process of homogeneous condensation is conventionally divided into two stages: the formation of condensation nuclei (of critical size) and the growth of these nuclei. The mass condensed per unit time is determined by the relation

$$\dot{m} = (1 - Y) J \rho_l \frac{4\pi r_c^3}{3} + 4\pi r^2 \frac{dr}{dt} \rho_l N, \tag{3}$$

Where J – the nucleation rate; $\frac{dr}{dt}$ – the droplet growth rate; ρ_l – the density of water; r_c – the critical radius; N – the number of water droplets per unit mass of moist vapor with radius r, and Y – the humidity.

Equations (2) assume that the liquid and gaseous phases move with the same velocity. This assumption is justified by the very small size of the water droplets. The liquid phase can be treated as a continuum consisting of a large number of water droplets contained in moist air-droplet flows. Due to the absence of slip between the vapor and water droplets, separate momentum equations for these droplets are not required. Two additional conservation equations are used to describe the liquid phase.

The nucleation rate J and the droplet growth rate $\frac{dr}{dt}$ are determined according to classical nucleation theory [4].

The flux of moisture impinging on a streamlined surface can be calculated using the relation:

$$q = \frac{k}{(1 - 0.4k)\sqrt{2\pi R_g}} \left(\frac{P_g}{\sqrt{T_g}} - \frac{P_s}{\sqrt{T_s}} \right), \tag{4}$$

where $0 < k < 1$ – the condensation coefficient of the vapor, R_g – the specific gas constant for the vapor, T_g and T_s – the temperatures of the vapor and the condensate surface, respectively, P_g – the saturation pressure of the vapor at temperatura T_g, P_s – the saturation pressure at temperature T_s.

It should be noted that the homogeneous model can be applied to icing problems in cases where bodies are exposed to moist flow under conditions with temperatures close to the phase transition temperature. In such cases, the freezing of surface moisture is primarily determined by the lower temperature of the streamlined body and by heat removal from the condensation surface due to evaporation.

2.2 Lagrangian trajectory model

Until now, the Lagrangian trajectory model has been the most widely applied in methodologies for simulating aircraft icing processes. Within this framework, numerical modeling can be performed by solving the Navier–Stokes equations together with the continuity and energy conservation equations in curvilinear coordinates (1), where

$$\hat{\mathrm{q}} = \frac{1}{J}\begin{bmatrix} \rho \\ \rho u \\ \rho v \\ \rho w \\ e \end{bmatrix}, \qquad \hat{\mathrm{E}} = \frac{1}{J}\begin{bmatrix} \rho U \\ \rho U u + \xi_x p \\ \rho U v + \xi_y p \\ \rho U w + \xi_z p \\ (e+p)U \end{bmatrix}, \qquad \hat{\mathrm{F}} = \frac{1}{J}\begin{bmatrix} \rho V \\ \rho V u + \eta_x p \\ \rho V v + \eta_y pc \\ \rho V w + \eta_z p \\ (e+p)V \end{bmatrix},$$

$$\hat{\mathrm{G}} = \frac{1}{J}\begin{bmatrix} \rho W \\ \rho W u + \zeta_x p \\ \rho W v + \zeta_y p \\ \rho W w + \zeta_z p \\ (e+p)W \end{bmatrix}, \qquad \hat{\mathrm{H}} = \frac{1}{J}\begin{bmatrix} 0 \\ 0 \\ 0 \\ 0 \\ 0 \end{bmatrix},$$

$$\hat{\mathrm{R}} = \frac{1}{J}\begin{bmatrix} 0 \\ \mu\left(\xi_x^2+\xi_y^2+\xi_z^2\right)u_\xi + \left(\frac{\mu}{3}\right)\xi_x\left(\xi_x u_\xi + \xi_y v_\xi + \xi_z w_\xi\right) \\ \mu\left(\xi_x^2+\xi_y^2+\xi_z^2\right)v_\xi + \left(\frac{\mu}{3}\right)\xi_y\left(\xi_x u_\xi + \xi_y v_\xi + \xi_z w_\xi\right) \\ \mu\left(\xi_x^2+\xi_y^2+\xi_z^2\right)w_\xi + \left(\frac{\mu}{3}\right)\xi_z\left(\xi_x u_\xi + \xi_y v_\xi + \xi_z w_\xi\right) \\ \frac{k}{\mathrm{Pr}(\gamma-1)}\left(\xi_x^2+\xi_y^2+\xi_z^2\right)\frac{\partial}{\partial\xi}\left(a^2\right) + \\ +\frac{\mu}{2}\left(\xi_x^2+\xi_y^2+\xi_z^2\right)\left(u^2+v^2+w^2\right)_\xi + \\ +\frac{\mu}{6}\left[\xi_x^2\left(u^2\right)_\xi + \xi_y^2\left(v^2\right)_\xi + \xi_z^2\left(w^2\right)_\xi + 2\xi_x\xi_y\left(uv\right)_\xi\right] \end{bmatrix}, \quad \hat{\mathrm{S}} = \frac{1}{J}\begin{bmatrix} 0 \\ \mu\left(\eta_x^2+\eta_y^2+\eta_z^2\right)u_\eta + \left(\frac{\mu}{3}\right)\eta_x\left(\eta_x u_\eta + \eta_y v_\eta + \eta_z w_\eta\right) \\ \mu\left(\eta_x^2+\eta_y^2+\eta_z^2\right)v_\eta + \left(\frac{\mu}{3}\right)\eta_y\left(\eta_x u_\eta + \eta_y v_\eta + \eta_z w_\eta\right) \\ \mu\left(\eta_x^2+\eta_y^2+\eta_z^2\right)w_\eta + \left(\frac{\mu}{3}\right)\eta_z\left(\eta_x u_\eta + \eta_y v_\eta + \eta_z w_\eta\right) \\ \frac{k}{\mathrm{Pr}(\gamma-1)}\left(\eta_x^2+\eta_y^2+\eta_z^2\right)\frac{\partial}{\partial\eta}\left(a^2\right) + \\ +\frac{\mu}{2}\left(\eta_x^2+\eta_y^2+\eta_z^2\right)\left(u^2+v^2+w^2\right)_\eta + \\ +\frac{\mu}{6}\left[\eta_x^2\left(u^2\right)_\eta + \eta_y^2\left(v^2\right)_\eta + \eta_z^2\left(w^2\right)_\eta + 2\eta_x\eta_y\left(uv\right)_\eta\right] \end{bmatrix}, \tag{5}$$

$$\hat{\mathrm{T}} = \frac{1}{J}\begin{bmatrix} 0 \\ \mu\left(\zeta_x^2+\zeta_y^2+\zeta_z^2\right)u_\zeta + \left(\frac{\mu}{3}\right)\zeta_x\left(\zeta_x u_\zeta + \zeta_y v_\zeta + \zeta_z w_\zeta\right) \\ \mu\left(\zeta_x^2+\zeta_y^2+\zeta_z^2\right)v_\zeta + \left(\frac{\mu}{3}\right)\zeta_y\left(\zeta_x u_\zeta + \zeta_y v_\zeta + \zeta_z w_\zeta\right) \\ \mu\left(\zeta_x^2+\zeta_y^2+\zeta_z^2\right)w_\zeta + \left(\frac{\mu}{3}\right)\zeta_z\left(\zeta_x u_\zeta + \zeta_y v_\zeta + \zeta_z w_\zeta\right) \\ \frac{k}{\mathrm{Pr}(\gamma-1)}\left(\zeta_x^2+\zeta_y^2+\zeta_z^2\right)\frac{\partial}{\partial\zeta}\left(a^2\right) + \\ +\frac{\mu}{2}\left(\zeta_x^2+\zeta_y^2+\zeta_z^2\right)\left(u^2+v^2+w^2\right)_\zeta + \\ +\frac{\mu}{6}\left[\zeta_x^2\left(u^2\right)_\zeta + \zeta_y^2\left(v^2\right)_\zeta + \zeta_z^2\left(w^2\right)_\xi + 2\zeta_x\zeta_y\left(uv\right)_\zeta\right] \end{bmatrix}.$$

Assuming that a droplet is a rigid sphere, it is considered that the forces acting on it in the flow are aerodynamic drag and gravity. The motion of the droplet can then be described by the following equation [5]:

$$m_d \vec{a}_d = \frac{C_d}{2} \rho_a A_d \left\| \vec{V}_r \right\| \vec{V}_r + m_g \vec{g}, \tag{6}$$

where $\vec{a}_d$ – the droplet acceleration, m_d – the droplet mass, A_d – the characteristic droplet area, $\vec{g}$ – the gravitational force vector, ρ_a – the air density, and $\vec{V}_r$ – the droplet velocity relative to the air. The drag coefficient C_d is a function of the droplet Reynolds number:

$$\mathrm{Re}_d = \frac{\left\| \vec{V}_r \right\| d}{\nu}. \tag{7}$$

Using this model, droplet trajectories can be computed by integrating Equation (6).

The flux of liquid impinging on a streamlined surface is determined by the product of the collection efficiency, the liquid water content, and the freestream velocity. Initially, a droplet release region is defined upstream (a vertical rectangular grid) covering the target area, with a specified minimum cell size. Droplets are released from the grid vertices, their trajectories are calculated, and the impact points on the surface are determined. The collection efficiency for a surface element can be computed as the ratio of the area of the rectangle from which droplets are released to the area of the quadrilateral formed by the impact points, or alternatively, as the number of droplets striking the surface element multiplied by the minimum upstream cell area and divided by the surface element area [6].

It should be noted that the Lagrangian trajectory model has several limitations that become critical for three-dimensional problems. Significant challenges arise when dealing with complex geometries, such as non-axisymmetric nacelles, wings with high-lift devices, air intakes, and systems with internal and external flows, because a large number of trajectories must be calculated, making the model computationally expensive. Additional difficulties and limitations occur in defining droplet release regions, specifying impact boundaries, and determining the spatial distribution of the collection efficiency on the surface.

2.3 Polydisperse Eulerian model

The polydisperse Eulerian model is based on the concept of a multi-velocity, multi-temperature medium, in which each point contains as many velocities and temperatures as there are phases in the considered medium. It is assumed that each phase continuously fills the space.

The equations describing the carrier air flow and the supercooled water droplets are coupled through source terms that account for interphase momentum and energy exchange. These equations differ from the Navier–Stokes equations only by the presence of these source terms. To determine the components describing interphase interaction, results from studies of particle-gas flow interactions were used.

The unsteady equations of the two-phase flow in a three-dimensional formulation have the form (1), where

$$\hat{q}=\frac{1}{J}\begin{bmatrix}\rho\\ \rho u\\ \rho v\\ \rho w\\ e\\ \rho_{jk}\\ \rho_{jk}u_{jk}\\ \rho_{jk}v_{jk}\\ \rho_{jk}w_{jk}\\ e_{jk}\end{bmatrix},\quad \hat{E}=\frac{1}{J}\begin{bmatrix}\rho U\\ \rho Uu+\xi_x p\\ \rho Uv+\xi_y p\\ \rho Uw+\xi_z p\\ (e+p)U\\ \rho_{jk}U_{jk}\\ \rho_{jk}U_{jk}u_{jk}\\ \rho_{jk}U_{jk}v_{jk}\\ \rho_{jk}U_{jk}w_{jk}\\ e_{jk}U_{jk}\end{bmatrix},\quad \hat{F}=\frac{1}{J}\begin{bmatrix}\rho V\\ \rho Vu+\eta_x p\\ \rho Vv+\eta_y p\\ \rho Vw+\eta_z p\\ (e+p)V\\ \rho_{jk}V_{jk}\\ \rho_{jk}V_{jk}u_{jk}\\ \rho_{jk}V_{jk}v_{jk}\\ \rho_{jk}V_{jk}w_{jk}\\ e_{jk}V_{jk}\end{bmatrix},\quad \hat{G}=\frac{1}{J}\begin{bmatrix}\rho W\\ \rho Wu+\zeta_x p\\ \rho Wv+\zeta_y p\\ \rho Ww+\zeta_z p\\ (e+p)W\\ \rho_{jk}W_{jk}\\ \rho_{jk}W_{jk}u_{jk}\\ \rho_{jk}W_{jk}v_{jk}\\ \rho_{jk}W_{jk}w_{jk}\\ e_{jk}W_{jk}\end{bmatrix},\quad \hat{H}=\frac{1}{J}\begin{bmatrix}0\\ H_u\\ H_v\\ H_w\\ H_e\\ 0\\ -H_{uk}\\ -H_{vk}\\ -H_{wk}\\ -H_{ek}\end{bmatrix},$$

$$\hat{R}=\frac{1}{J}\begin{bmatrix}0\\ \mu\left(\xi_x^2+\xi_y^2+\xi_z^2\right)u_\xi+\left(\frac{\mu}{3}\right)\xi_x\left(\xi_x u_\xi+\xi_y v_\xi+\xi_z w_\xi\right)\\ \mu\left(\xi_x^2+\xi_y^2+\xi_z^2\right)v_\xi+\left(\frac{\mu}{3}\right)\xi_y\left(\xi_x u_\xi+\xi_y v_\xi+\xi_z w_\xi\right)\\ \mu\left(\xi_x^2+\xi_y^2+\xi_z^2\right)w_\xi+\left(\frac{\mu}{3}\right)\xi_z\left(\xi_x u_\xi+\xi_y v_\xi+\xi_z w_\xi\right)\\ \frac{k}{\Pr(\gamma-1)}\left(\xi_x^2+\xi_y^2+\xi_z^2\right)\frac{\partial}{\partial\xi}\left(a^2\right)+\\ +\frac{\mu}{2}\left(\xi_x^2+\xi_y^2+\xi_z^2\right)\left(u^2+v^2+w^2\right)_\xi+\\ +\frac{\mu}{6}\left[\xi_x^2\left(u^2\right)_\xi+\xi_y^2\left(v^2\right)_\xi+\xi_z^2\left(w^2\right)_\xi+2\xi_x\xi_y(uv)_\xi\right]\\ 0\\ 0\\ 0\\ 0\end{bmatrix},\quad \hat{S}=\frac{1}{J}\begin{bmatrix}0\\ \mu\left(\eta_x^2+\eta_y^2+\eta_z^2\right)u_\eta+\left(\frac{\mu}{3}\right)\eta_x\left(\eta_x u_\eta+\eta_y v_\eta+\eta_z w_\eta\right)\\ \mu\left(\eta_x^2+\eta_y^2+\eta_z^2\right)v_\eta+\left(\frac{\mu}{3}\right)\eta_y\left(\eta_x u_\eta+\eta_y v_\eta+\eta_z w_\eta\right)\\ \mu\left(\eta_x^2+\eta_y^2+\eta_z^2\right)w_\eta+\left(\frac{\mu}{3}\right)\eta_z\left(\eta_x u_\eta+\eta_y v_\eta+\eta_z w_\eta\right)\\ \frac{k}{\Pr(\gamma-1)}\left(\eta_x^2+\eta_y^2+\eta_z^2\right)\frac{\partial}{\partial\eta}\left(a^2\right)+\\ +\frac{\mu}{2}\left(\eta_x^2+\eta_y^2+\eta_z^2\right)\left(u^2+v^2+w^2\right)_\eta+\\ +\frac{\mu}{6}\left[\eta_x^2\left(u^2\right)_\eta+\eta_y^2\left(v^2\right)_\eta+\eta_z^2\left(w^2\right)_\eta+2\eta_x\eta_y(uv)_\eta\right]\\ 0\\ 0\\ 0\\ 0\end{bmatrix}, \tag{8}$$

$$\hat{T}=\frac{1}{J}\begin{bmatrix}0\\ \mu\left(\zeta_x^2+\zeta_y^2+\zeta_z^2\right)u_\zeta+\left(\frac{\mu}{3}\right)\zeta_x\left(\zeta_x u_\zeta+\zeta_y v_\zeta+\zeta_z w_\zeta\right)\\ \mu\left(\zeta_x^2+\zeta_y^2+\zeta_z^2\right)v_\zeta+\left(\frac{\mu}{3}\right)\zeta_y\left(\zeta_x u_\zeta+\zeta_y v_\zeta+\zeta_z w_\zeta\right)\\ \mu\left(\zeta_x^2+\zeta_y^2+\zeta_z^2\right)w_\zeta+\left(\frac{\mu}{3}\right)\zeta_z\left(\zeta_x u_\zeta+\zeta_y v_\zeta+\zeta_z w_\zeta\right)\\ \frac{k}{\Pr(\gamma-1)}\left(\zeta_x^2+\zeta_y^2+\zeta_z^2\right)\frac{\partial}{\partial\zeta}\left(a^2\right)+\\ +\frac{\mu}{2}\left(\zeta_x^2+\zeta_y^2+\zeta_z^2\right)\left(u^2+v^2+w^2\right)_\zeta+\\ +\frac{\mu}{6}\left[\zeta_x^2\left(u^2\right)_\zeta+\zeta_y^2\left(v^2\right)_\zeta+\zeta_z^2\left(w^2\right)_\xi+2\zeta_x\zeta_y(uv)_\zeta\right]\\ 0\\ 0\\ 0\\ 0\end{bmatrix},$$

$$e = \rho\left[\varepsilon + \frac{1}{2}\left(u^2 + v^2 + w^2\right)\right],$$
$$e_{jk} = \gamma\rho_{jk}\left[\omega T_{jk} + \left(u_{jk}^2 + v_{jk}^2 + w_{jk}^2\right)\right]. \quad (9)$$

The main assumptions of the model are as follows:

- The medium is multi-velocity and multi-temperature, consisting of air—a viscous compressible carrier gas—and supercooled droplets, which are fractions with a specified size distribution, treated as incompressible spherical particles that do not interact with each other.
- The specific heats of air and supercooled droplets are constant.
- The droplet sizes are much larger than molecular-kinetic scales and much smaller than the characteristic distances over which the averaged macroscopic flow parameters change significantly.
- The interaction between supercooled droplets and air occurs through gas viscosity.
- The temperature of an individual supercooled droplet is uniform throughout its volume.

In equations (8–9), the following notations are used: a – speed of sound; γ – ratio of specific heats; μ – dynamic viscosity coefficient; Re – Reynolds number; Pr – Prandtl number; variables with subscript *j* describe the droplets; ω – ratio of the specific heat of droplets to that of air at constant pressure; subscript *k* varies from 1 to *n*, where *n* is the number of intervals corresponding to the mass fractions of droplets of a given size in the air-droplet flow (according to the adopted droplet size distribution law in the cloud volume).

The intensity of interphase momentum and energy exchange is determined by the following expressions [7]:

$$H_{uk} = \rho_{jk} A_{jk}\left(u - u_{jk}\right),\ H_{vk} = \rho_{jk} A_{jk}\left(v - v_{jk}\right),$$
$$H_{wk} = \rho_{jk} A_{jk}\left(w - w_{jk}\right), H_{ek} = \rho_{jk} A_{jk} B_{jk}, \quad (10)$$
$$H_u = \sum_{k=1}^{n} H_{uk},\ H_v = \sum_{k=1}^{n} H_{vk},\ H_w = \sum_{k=1}^{n} H_{wk},\ H_e = \sum_{k=1}^{n} H_{ek},$$

where A_{jk}, B_{jk} – are coefficients defining the exchange of momentum and energy between phases.

The initial distribution of droplet concentration in the air-droplet flow corresponding to the *k*-th interval is given by:

$$\rho_{jk} = \rho\phi_k / \left(1 - \phi_k\right), \quad (11)$$

where $\phi_k = W_{jk} / W_m$ – the mass fraction of droplets in the air-droplet flow that fall within the *k*-th interval, and, $\rho_j = \sum_{k=1}^{n} \rho_{jk}$ – the total droplet concentration at the surface of the streamlined body.

The moisture flux impinging on the streamlined surface, when applying the interpenetrating media (homogeneous) model, can be calculated as:

$$q = \sum_{k=1}^{n} (\rho_{jk} U_{jnk}), \tag{12}$$

where ρ_{jk} – the concentration of supercooled droplets in the air-droplet flow near the body surface corresponding to the *k*-th size interval, U_{jnk} – the droplet velocity component normal to the surface for the *k*-th interval, and n is the total number of size intervals.

The Lagrangian trajectory and the polydisperse Eulerian models are most suitable when the airflow contains relatively large (sufficiently inertial) supercooled water droplets, which play the primary role in the deposition of moisture on the streamlined surface.

2.4. Solution Technique

The discretization of the Reynolds-averaged Navier-Stokes equations is performed using an implicit finite-volume method. To calculate the convective terms, we used the scheme Roe [8]. The viscous terms are approximated by a three-point pattern with a second order of accuracy. The block-matrix system of algebraic equations is solved by the iterative Gauss-Seidel algorithm.

In turbulence modeling, the one-parameter differential Spalart-Allmaras model [9] with a correction for a rough wall [10] and the detached eddy simulation method DES [11] are used.

3 THE MODEL OF ICE GROWTH

To describe the process of ice growth, the surface control volume method was used. Equations of mass and energy balance for the control volume can be obtained from the laws of conservation of mass, energy, and momentum applied to a control volume defined on the surface of the body [12,13].

Mass balance equation. Let us consider a control volume defined on the surface of an airfoil or streamlined body. The mass of water entering the control volume during the considered period of time consists of the sum of three masses of water in the liquid state – the mass of the incoming water from the external stream in the form of supercooled droplets m_{cap}, the mass of incoming water from the previous control volume m_{rbin} and the mass of the remaining liquid water from the previous time step m_{resw}:

$$m_{in} = m_{cap} + m_{rbin} + m_{resw}. \tag{13}$$

The mass of water from the external stream corresponds to the fraction of supercooled droplets in the incoming air-droplet flow that impinges on the surface:

$$m_{cap} = \rho_j \cdot U_{jn} \cdot \Delta b \cdot \Delta s \cdot \Delta t_{acc}, \tag{14}$$

where ρ_j – the concentration of particles at the surface of the body, U_{jn} – the component of the velocity of the disperse phase normal to the streamlined surface, Δb, Δs – the width and length of the control volume, Δt_{acc} – a time increment of the icing process.

Mass of incoming water m_{rbin} is a share of water mass in a liquid state m_{rbout} from a previous control volume, denoted as *i-1*, drawing into the current control volume, denoted as *i,* external flow:

$$m_{rbin(i)} = m_{rbout(i-1)}. \tag{15}$$

The mass of residual water is equal to the mass of residual liquid water m_{rmw}, which was determined in this control volume at the previous time step:

$$m_{resw}^{t} = m_{rmw}^{t-\Delta t}. \tag{16}$$

On the other hand, the mass of water m_{in} entering the control volume is consumed by the mass of the leaving water m_{out}, the residual water mass m_{rmw} and the residual ice mass m_{rmi}:

$$m_{in} = m_{out} + m_{rmw} + m_{rmi}. \tag{17}$$

The mass of water leaving the volume includes contributions in the solid, liquid, and vapor phases. It consists of five components: the mass of sublimated ice m_{sub}, the mass of evaporated water m_{evap}, the mass of liquid water coming out of the volume m_{rbout}, the mass of the liquid water dragged by the flow m_{shw}, and the mass of the ice dragged by the flow m_{shi}:

$$m_{out} = m_{sub} + m_{evap} + m_{rbout} + m_{shw} + m_{shi}. \tag{18}$$

The mass of sublimated ice and the mass of evaporated water are parts of the ice mass and the mass of water in the liquid state that evaporate into the air under the influence of temperature differences in the boundary layer. The mass of the water leaving the volume in the liquid state is part of the mass of water in the control volume, which is transferred to the next control volume. The mass of shedding water in a liquid state is part of the mass of water inside the control volume that is released into the air under the action of shearing stresses caused by the oncoming flow. It can be determined by the Weber number, using the empirical relationship [13]. In the presence of flow separation, which is determined from the calculation of an external compressible viscous flow, we assume that all unfrozen water leaving the previous control volume is splashed and carried away by an external flow. The mass of the ice dragged away is part of the ice mass in the control volume, which is thrown into the air due to the detachment of ice crystals under the influence of aerodynamic force.

Heat balance equation. From the energy conservation equation for the control volume, one can obtain the heat balance equation having the form:

$$Q_f + Q_{ss} + Q_{sub} + Q_{evap} + Q_{adh} + Q_{kin} + Q_{cd} + Q_{cv} + Q_{rad} = 0, \tag{19}$$

where Q_f is the phase transition latent heat, Q_{sub} is the latent heat of sublimation, Q_{evap} is the latent heat of evaporation, Q_{ss} is the internal heat, Q_{cv} is the heat transfer by convection, Q_{cd} is the heat transfer by conduction, Q_{rad} is the heat exchange by radiation, Q_{adh} is the aerodynamic heat, Q_{kin} is the kinetic heat.

On the basis of mass and heat balances, the frozen fraction f of water passing through the control volume during the time Δt_{acc} is calculated.

4 TEST CASE

To validate the proposed methodology for modeling air-droplet flow and icing processes, a numerical simulation of the NACA 0012 airfoil icing was performed. The airfoil had a chord of L = 0.3 m and was set at zero angle of attack (α = 0°). The simulation conditions

corresponded to typical glaze ice formation studied in wind tunnels such as the NASA Glenn Icing Research Tunnel (IRT) [13]. Specifically, the incoming flow speed was $V_\infty = 129.46$ m/s, the temperature $T_\infty = -12.6$°C, the pressure $p_\infty = 9.075 \times 10^4$ Pa, the liquid water content LWC = 1.0 g/m³, and the median volume diameter of the droplets MVD = 20 μm. Additionally, the airfoil surface roughness, represented by an equivalent sand-grain roughness $k_s = 0.00020$ m, was taken into account, which is important for accurate prediction of aerodynamic characteristics.

The simulation results were compared with published computational and experimental data (Fig. 1) [13]. The predicted ice shape demonstrates the characteristic features of glaze ice, with maximum ice thickness at the leading edge and horn-like protrusions extending into the flow. The distribution of Mach number isolines near the airfoil, also shown in Fig. 1, reflects the influence of ice growth on the aerodynamic flow, in particular local velocity variations caused by modifications of the surface geometry.

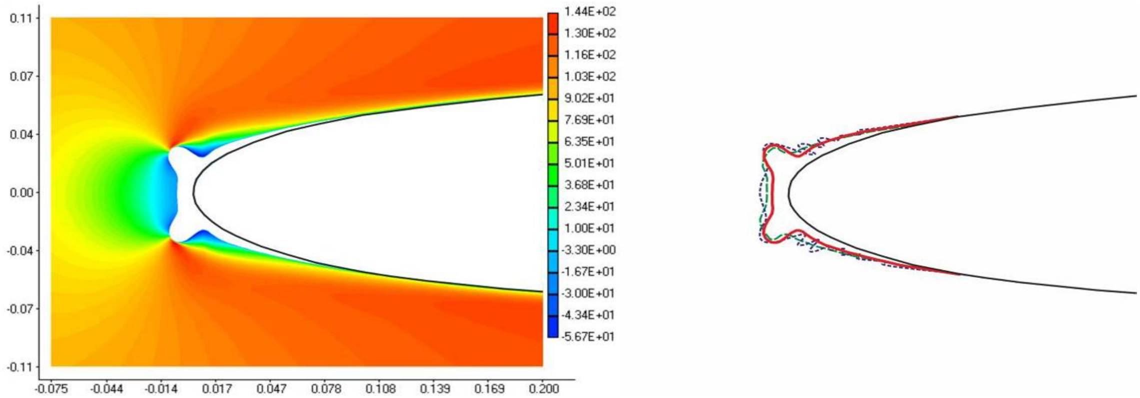

- calculation of the given work, - LEWICE 1.6 calculations [13], - experimental data [13]

Fig. 1 Ice accretion shape, Mach number isolines distribution near NACA 0012 profile (α= 0°)

5 CONCLUSIONS

– The analysis has shown that, for modeling air-droplet flow in aircraft icing problems, the polydisperse Eulerian model is the most promising. It effectively accounts for the two-phase viscous compressible flow, droplet polydispersity, and interphase exchange of momentum and energy, which is critically important for complex three-dimensional geometries. The homogeneous model is suitable for conditions close to phase transition, where condensation dominates, but it is limited for inertial supercooled droplets. The Lagrangian trajectory model provides accurate droplet trajectories but is computationally expensive in 3D applications due to the large number of trajectories required and the complexity of determining impingement zones.

– The proposed approach enables accurate prediction of droplet impingement locations and ice accretion dynamics. A test case on the NACA 0012 airfoil (MVD = 20 μm, LWC = 1.0 g/m³) demonstrated good agreement with available experimental data for ice shapes, confirming the applicability of the method for anti-icing system design and flight safety assessment.

6 ACKNOWLEDGMENTS

The work was carried out with the financial support of the Ministry of Education and Science within the framework of international scientific and technological cooperation in accordance with the Protocol of the Fifteenth Meeting of the Joint Ukraine-NATO Working Group on Cooperation in Science and the Environment dated July 4, 2017 and the letter of the Dnipro University of Technology dated January 6, 2025 No. 01-29/4, regarding the provision of funding for research work under the project of the NATO Program "Science for Peace and Security".

REFERENCES

[1] Alekseenko, S.V., Prikhod'ko, A.A. Mathematical modeling of ice body formation on the wing airfoil surface. *Fluid Dynamics* (2014) 49(6):715–732.
[2] Dykas, S. Numerical calculation of the stream condensing flow. *CFD for Turbomachinery Applications 2001*, Gdansk (2001) K10:11.
[3] Liang, L., Guojun, L., Zhenping, F. Numerical simulation of spontaneously condensing flows in a plane turbine cascade. *CFD for Turbomachinery Applications 2001*, Gdansk (2001) C21:7.
[4] Prykhodko, O.A., Alekseyenko, S.V. Numerical simulation of the process of airfoil icing in the presence of large supercooled water drops. *Technical Physics Letters* (2014) 40:864–867.
[5] Ruff, G.A., Berkowitz, B.M. *Users Manual for the NASA Lewis Ice Accretion Prediction Code (LEWICE)*. NASA Contractor Report 185129 (1990).
[6] Bidwell, C., Pinella, D., Garrison, P. Ice accretion calculations for a commercial transport using the LEWICE3D, ICEGRID3D and CMARC programs. AIAA Paper 99-0250, Reno (1999).
[7] Chang, I.-S. One- and two-phase nozzle flows. *AIAA Journal* (1980) 18(12):1455–1461.
[8] Roe, P.L. Characteristic-based schemes for the Euler equations. *Annual Review of Fluid Mechanics* (1986) 18:337–365.
[9] Spalart, P.R., Allmaras, S.R. A one-equation turbulence model for aerodynamic flows. AIAA Paper 92-0439 (1992) 22.
[10] Aupoix, B., Spalart, P.R. Extensions of the Spalart-Allmaras turbulence model to account for wall roughness. *International Journal of Heat and Fluid Flow* (2003) 24:454–462.
[11] Constantinescu, G.S., Chapelet, M.C., Squires, K.D. Turbulence modeling applied to flow over a sphere. *AIAA Journal* (2003) 41(9):1733–1743.
[12] Louchez, P., Fortin, G., Mingione, G., Brandi, V. Beads and rivulets modelling in ice accretion on a wing. *36th Aerospace Sciences Meeting & Exhibit*, AIAA, Reno, Nevada (1998) 1055.
[13] Wright, W.B. *Users Manual for the Improved NASA Lewis Ice Accretion Code LEWICE 1.6*. NASA Contractor Report (1995) 95.